

One Latent Space to Rule All Degradations: Unifying Restoration Knowledge for Image Fusion

Haolong Ma
Jiangnan University

Hui Li
Jiangnan University

Chunyang Cheng
Jiangnan University

Zeyang Zhang
Jiangnan University

Xiaoqing Luo
Jiangnan University

Zhongwei Shen
Suzhou University of Science and Technology

Xiaoning Song
Jiangnan University

Xiao-Jun Wu
Jiangnan University

Abstract

All-in-One Degradation-Aware Fusion Models (ADFM) as one of multi-modal image fusion models, which aims to address complex scenes by mitigating degradations from source images and generating high-quality fused images. Mainstream ADFMs rely on end-to-end learning and heavily synthesized datasets to achieve degradation awareness and fusion. This rough learning strategy and non-real world scenario dataset dependence often limit their upper-bound performance, leading to low-quality results. To address these limitations, we present LURE, a Learning-driven Unified REpresentation model for infrared and visible image fusion, which is degradation-aware. LURE learns a Unified Latent Feature Space (ULFS) to avoid the dependency on complex data formats inherent in previous end-to-end learning pipelines. It further improves image fusion quality by leveraging the intrinsic relationships between multi-modalities. A novel loss function is also proposed to drive the learning of unified latent representations more stable. More importantly, LURE seamlessly incorporates existing high-quality real-world image restoration datasets. To further enhance the model’s representation capability, we design a simple yet effective structure, termed internal residual block, to facilitate the learning of latent features. Experiments show our method outperforms state-of-the-art (SOTA) methods across general fusion, degradation-aware fusion, and downstream tasks. The code is available in the supplementary materials.

1. Introduction

Multi-modal image fusion, aims at creating high-quality fused images by integrating multi-modal sensor data; no-

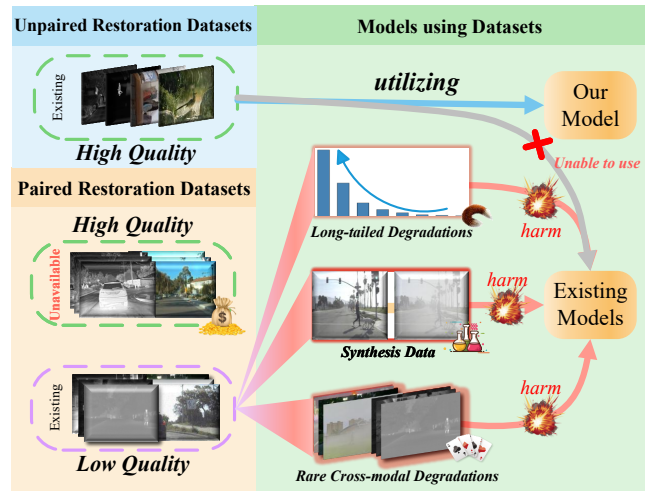


Figure 1. Illustration of the limitations in existing methods due to data-level issues. “Paired” denotes datasets containing corresponding infrared–visible image pairs.

tably, infrared and visible image fusion is recognized as one of its crucial tasks [6, 18, 61]. It faces challenges due to degradations in visual information of different modalities. Detailed visible images degrade under varying weather and lighting, causing information loss. In contrast, infrared images, capturing thermal radiation in adverse environments, typically have lower resolution/contrast.[32, 56, 58]. Thus, effective degradation removal and complementary data integration are essential for accurate scene reconstruction [9].

Conventional two-step methods first restore and then fuse modalities [56], but suffer from domain shift between restoration and fusion. Moreover, diverse degradation combinations (e.g., visible low light and infrared low contrast) make separate fusion training infeasible [10, 27, 62].

Current methods address this problem in one step by training an All-in-One degradation-aware fusion model (ADFM). Mainstream ADFMs typically employ a supervised paradigm, relying on high-quality paired infrared and visible images as explicit supervisory signals to achieve high-quality fusion [11, 56]. This means that each training sample for these methods consists of a quadruplet of four images: two low-quality images of the same scene as input, and two corresponding high-quality images as supervision signals for end-to-end learning [56] [53] [17] [15]. However, the datasets currently available to support the training of such fusion methods suffer from several critical deficiencies, which in turn constrain the fusion quality of existing models.

As illustrated in Fig.1, the infrared and visible modalities exhibit distinct types of degradation. These degradations are combined within the quadruplets required for training. Assuming there are M types of degradation in the infrared modality and N types in the visible modality, a total of $M \times N$ types of quadruplets would be necessary for comprehensive training. This leads to a combinatorial explosion and significantly increases the difficulty of dataset construction. Consequently, existing datasets heavily rely on synthetically generated data to simulate a wide array of degradation scenarios [53] [17] [15].

For existing IVIF datasets (e.g., RoadScene [54], MSRS [41], M3FD [33]), degraded images are typically handled through two strategies. The forward construction method restores degraded images using SOTA restoration techniques or manual adjustment to obtain ground truth, while the backward construction method artificially adds degradations to clean images when real degraded samples are scarce. Forward construction is limited by the scarcity of real degraded scenes. In contrast, backward construction often introduces a distribution gap from real degradations—especially for rare cases. Current datasets follow a long-tail distribution, with most samples covering common degradations (e.g., low light, overexposure) and only a few representing rare but critical ones (e.g., dense fog).

To address these issues, we propose a representation learning method based on decoupling. First, in the initial stage, we leverage existing high-quality image restoration datasets for each modality independently. The objective is to learn a unified latent representation space that is agnostic to the specific type of degradation. In this space, the original degradation type cannot be inferred from an image’s representation, making it degradation-agnostic. It serves as a unified representation where all degraded images are mapped, effectively eliminating the influence of specific degradations. In the second stage, we build upon the features from this representation space to learn how to generate high-quality fused results—that is, to learn the fusion rules. Since all types of degradation are mapped to

a common intermediate form, a single training process is sufficient to handle input images with any form of degradation. Importantly, for the first stage, we only require image restoration datasets, some of which provide high-quality supervision from real-world scenes (e.g., RESIDE [20], LOL [49]). For the second stage, we only need a standard image fusion dataset. This two-stage design enables us to circumvent the limitations of existing methods.

However, learning an effective image representation requires us to reconstruct the input image, ensuring that its representation preserves the critical information of the image. Existing image restoration models typically employ a skip connection [7] [57] [22] [8]. from input to output to accelerate model convergence, allowing the model to focus on the degraded regions of the image. While this architecture hinders the learning of a comprehensive image representation, removing it leads to slower convergence. Therefore, we adapt this residual learning mechanism by shifting from the conventional pixel-level residual to a feature-level residual, proposing an “inner residual structure” to resolve the aforementioned issue. The contributions of this paper can be summarized as follows:

- A novel data-decoupling and feature association method is proposed to address challenges in synthetic data over-reliance and jointly handle cross-model combined degradations.
- An efficient inner residual structure is introduced to enhance the model’s information retention while ensuring its ability to learn complete latent features.
- Extensive experiments are conducted. Results demonstrate the effectiveness of the proposed approach.

2. Related Work

2.1. Recent Image Fusion Methods

Mainstream image fusion models fall into three categories: generative models (e.g., FusionGAN, DDFM)[34, 35, 64], end-to-end approaches (e.g., U2Fusion)[29, 48, 63], and autoencoder-based methods (e.g., DenseFuse)[24–26]. Generative models fuse images via distribution approximation, yet face training instability and heuristic designs. End-to-end methods directly derive fused images, constrained by designed loss functions.

Despite stable training, their generalization is limited by handcrafted loss functions. Early autoencoders lacked adaptability with hand-engineered fusion strategies[24], whereas current methods use learnable rules for better adaptation [25]. Autoencoder methods inherently decouple fusion rule and feature learning, facilitating versatile, degradation-aware paradigms.

2.2. All-in-One Degradation-aware Models

All-in-One Degradation-aware Models (ADM) address diverse degradations within a single model[11, 22, 23]. In image restoration field, ADMs benefit from abundant high-quality datasets and use techniques like prompt/continual learning[1, 20, 49].

However, in image fusion field, ADFMs face challenges due to long-tailed degradation distributions in fusion datasets, lacking sufficient data for robust degradation restoration[33, 41, 54, 56]. Unsupervised methods like contrastive learning exist but often yield lower quality due to lacking explicit supervision[45]. Current ADFMs still rely on existing fusion dataset degradations or synthetic ones, which may not match real degradation distributions[45, 56]. Some degradations require extra modality information for realistic synthesis (e.g., fog needs depth maps), which is unavailable in current datasets.

These limitations hinder the generalization of current ADFMs. To address the above drawbacks, we propose a unified degradation-aware representation model to decouple image restoration and fusion data-level and re-associate them in latent space, which allows leveraging high-quality image restoration data to overcome current ADFMs challenges.

3. Proposed Method

3.1. Problem Formulation

In this paper, low/high-quality images are denoted by sets \mathcal{X}/\mathcal{Y} . Infrared/visible images are denoted by sets \mathcal{I}/\mathcal{V} .

Assume the set \mathcal{X} of T degradation types. For the t -th degradation ($t \in \{1, 2, \dots, T\}$), let c_t denote its description (e.g., text embedding), with $c_t \in \mathcal{C}$ and $\mathcal{C} = \{c_t\}_{t=1}^T$. Theoretically, for each image $x \in \mathcal{X}$, there exists a deterministic mapping to a corresponding degradation description c_t .

For supervised method, samples are quadruplets $(x_{ir}, y_{ir}, x_{vi}, y_{vi})$, where ir/vi denote infrared/visible modalities, and x/y are low/high-quality images. Define modality-paired sets: \mathcal{I}_g (infrared), \mathcal{V}_g (visible):

$$\mathcal{I}_g = \{(x_{ir}, y_{ir}) \mid x_{ir} \in \mathcal{X}, y_{ir} \in \mathcal{Y}, y_{ir} = f(x_{ir})\}, \quad (1)$$

where f maps low-quality images to clean counterparts. \mathcal{V}_g is defined analogously.

Given a sample $(x_{ir}, y_{ir}, x_{vi}, y_{vi})$ from the joint distribution $P_{\mathcal{I}_g, \mathcal{V}_g}(x_{ir}, y_{ir}, x_{vi}, y_{vi})$ and the description c , the loss function of existing supervised methods can be expressed as $\mathcal{L}_{if}(y_{ir}, y_{vi}, \mathcal{F}_{if}(x_{ir}, x_{vi}, c; \theta))$ where, \mathcal{L}_{if} is the fusion loss. \mathcal{F}_{if} is a network parameterized by θ , fusing degraded infrared and visible images with degradation description c .

Such supervised approaches necessitate quadruplet samples from the joint distribution of \mathcal{I}_g and \mathcal{V}_g to provide su-

pervision signals. This leads to the curse of dimensionality in handling combined degradations, fundamentally due to coupling modalities and quality dimensions at the data level.

3.2. Data Decoupling and Feature Association

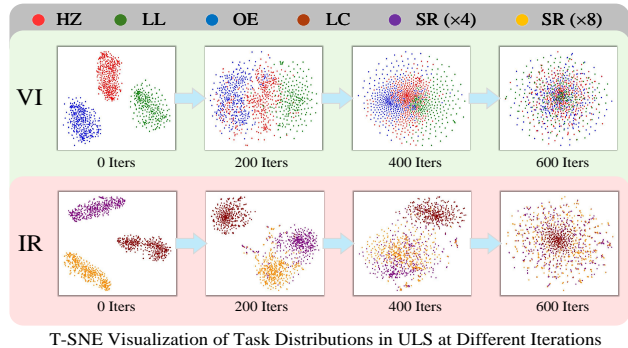


Figure 2. t-SNE visualization of ULFS distributions for tasks (e.g., HZ denotes Dehaze; other abbreviations are detailed in Sec.4.1.1.) of both modalities across training iterations. It reveals initial distinct task distributions gradually merging into a unified distribution. Detailed t-SNE visualizations are in the supplementary material.

To address modality-quality coupling in data-level, a novel decoupling mechanism which still preserves inherent associations of source data is needed. We thus propose a ULFS (\mathcal{Z}) to re-establish these associations at feature level. We define \mathcal{Z} as follows:

Definition: [Unified Latent Feature Space (\mathcal{Z})].

\mathcal{Z} is defined by mapping $f_e : \mathcal{X} \rightarrow \mathcal{Z}$, with conditions:

- (I) $\forall x \in \mathcal{X}, \exists z \in \mathcal{Z} (z = f_e(x))$.
- (II) $\forall z \in \mathcal{Z}, \forall c \in \mathcal{C} (P(c|z) = P(c))$.

1. Condition I ensures every degraded image maps to \mathcal{Z} .
2. Condition II ensures that for any latent feature $z \in \mathcal{Z}$, the posterior $P(c|z)$ distribution equals the prior $P(c)$ distribution for $c \in \mathcal{C}$.

Practically, each modality learns its own \mathcal{Z} for quality decoupling. These \mathcal{Z} properties guarantee f_e mapping eliminates unique degradation information. As shown in Fig.2, this ‘mixing’ of feature distributions in \mathcal{Z} renders degradations indistinguishable, allowing transfer of fusion rules across degradations.

We learn \mathcal{Z} for image quality using image restoration data at first stage. Then, at second stage, we learn a fusion rule in \mathcal{Z} using image fusion data.

3.2.1. Unified Latent Representation Learning

Theoretically, to align with the definition of \mathcal{Z} for ULFS learning, we aim to minimize the distribution distance of

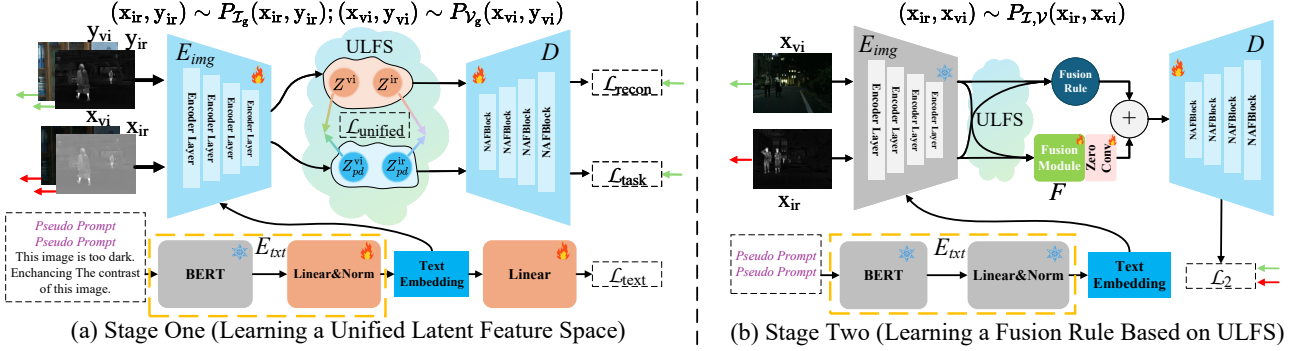


Figure 3. Two-stage training overview. (a) Stage I learns a unified latent space guided by text. (b) Stage II freezes encoders and trains a fusion module for strategy learning. “Pseudo prompt” denotes the prompt for pseudo degradation (details in Supplementary).

degraded images within \mathcal{Z} . Learning Objective:

$$\min_{\theta} \sum_{t=1}^T \sum_{t' \neq t}^T \text{KL}(P_{\mathcal{Z}}^{(t)}(z) \parallel P_{\mathcal{Z}}^{(t')}(z)), \quad (2)$$

where, $\text{KL}(\cdot \parallel \cdot)$ denotes the Kullback-Leibler divergence, and $P_{\mathcal{Z}}^{(t)}(z)$ represents the distribution of the t -th degradation in \mathcal{Z} .

To minimize Eq.2, Generative Adversarial Networks (GANs) with discriminators are commonly used for adversarial training [30, 38]. However, inherent distribution differences exist across image restoration datasets. As the discriminators tend to capture these discrepancies, the GAN training process becomes unstable and struggles to converge.

To mitigate this issue, we introduce a pseudo-degradation task. This task, fundamentally image reconstruction, is not a genuine degradation. For this task, pseudo-degradation data pairs (x, y) satisfy $x = y$, where $x \in \mathcal{X}$ and $y \in \mathcal{Y}$. We control this task via a description c_{pd} and align all degradation distributions to this pseudo-degradation task distribution.

For the t -th degradation, given an image restoration data pair (x_t, y_t) where $x_t \in \mathcal{X}$ and $y_t \in \mathcal{Y}$, we have $z_t = f_e(x_t, c_t)$. We construct a pseudo-task data pair (y_t, y_t) , yielding $z_{pd} = f_e(y_t, c_{pd})$.

Theoretically, z_{pd} should ideally correspond to z_t as a feature point in ULFS. This is justified by:

1. x_t and y_t represent the same scene information.
2. Pseudo-degradation, being image reconstruction of degradation-free y_t , results in $z_{pd} \in \mathcal{Z}$ lacking degradation information, thus obscuring original degradation types.

Therefore, to align distributions of tasks in \mathcal{Z} , we ensure each task’s representation aligns with its pseudo-task counterpart. We transform distribution alignment in the objective function to feature alignment:

$$\mathcal{L}_{\text{unified}} = \frac{1}{T} \sum_{t=1}^T \{1 - \Gamma[f_e(X_t, c_t), f_e(Y_t, c_{pd})]\}, \quad (3)$$

where, X_t and Y_t represent low-quality and high-quality image datasets for task t , respectively. Γ measures feature distances in \mathcal{Z} , employing cosine similarity.

It is worth emphasizing that, in practice, the distributional discrepancies among different datasets still prevent Condition II in the ULFS definition from being perfectly satisfied. Consequently, the learned latent space can only approximately meet this condition. Nevertheless, directly constraining feature relationships for \mathcal{Z} learning proves to be more stable than GAN-based adversarial approaches. The pseudo-task acts as an image auto-encoding process to learn the fusion rule in the second stage and to bridge the two stages at the feature level. In practice, f_e functions as a conditional image encoder.

3.3. Network Pipeline

3.3.1. Encoder and Decoder Structure

As shown in Fig.3 (a), the encoder is bifurcated into image (E_{img}) and text (E_{txt}) encoders. E_{txt} employs Distilled BERT [14], with a Norm layer and a Linear layer to project its final output into a text feature vector. A classification head and cross-entropy loss (\mathcal{L}_{txt}) are used to align task categories for each task-specific text feature vector, an approach effective in InstructIR [37] and superior to the CLIP text encoder [39].

E_{img} comprises multi-scale Encoder Layers for mapping and reconstructing input images to learn \mathcal{Z} . Unlike conventional restoration models using residual structures ($\hat{y} = \mathcal{M}(x) + x$) [7, 22, 57], which emphasize degraded-region correction over source reconstruction, our framework requires balanced feature learning. To avoid detail loss from removing the residual path, we introduce an inner residual structure to preserve fine information. Each Encoder Layer (Fig.4) includes four modules—BaseBlock, TGABlock (Text-Guided Attention Block), BottleNeck, and Linear—where TGABlock is integrated with BaseBlock and BottleNeck to form two composite units, iterated K_{tb}^i and K_{tb}^i times in the i -th layer.

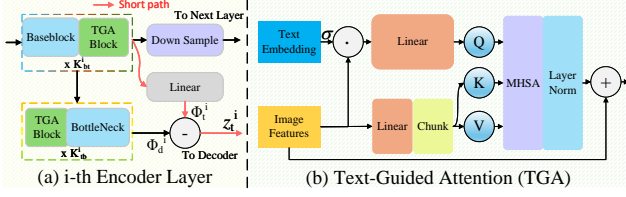


Figure 4. Schematic diagrams of Encoder Layer and Text-Guided Attention (TGA). (a) Structure diagram of the Encoder Layer. (b) Structure diagram of TGA. “ \odot , \oplus , \ominus ” represent Element-wise operations, and σ represents the Sigmoid function.

As shown in Fig.4, at the i -th layer, TGABlock + BaseBlock extract modality-specific features and integrate degradation information guided by text. The output branches into three paths: (1) downsampling to the next layer, (2) TGABlock + BottleNeck for degradation-specific feature extraction Φ_d^i , and (3) a linear layer for task-relevant base information Φ_t^i . A residual subtraction yields task-irrelevant latent representations $z_t^i = \Phi_t^i - \Phi_d^i$, providing a shorter decoding path and mitigating detail loss.

BaseBlock (NAFBlock [7] + Modality Embedding) extracts modality-aware basic features, while BottleNeck (NAFBlock + 1×1 conv) retains text-relevant cues and reduces redundancy. The TGABlock adopts a Transformer-like design with GDFN [57] as its feed-forward block. Unlike passive channel-weighting schemes [37, 56], TGABlock employs channel-weighted text features as Queries to actively attend to global image features, enhancing text-guided spatial awareness and preserving task-related details.

Each decoder layer then upsamples and refines details from \mathcal{Z} using a few NAFBlocks, while the fusion stage incorporates multi-scale Cross Attention modules for effective multimodal interaction.

3.3.2. Training

In our proposed framework, the training processing is a two-stage scheme. As shown in Fig.3 (a), in the first stage, the latent space \mathcal{Z} is learned. For each sample, we have $(x_{ir}, y_{ir}) \sim P_{\mathcal{I}_g}(x_{ir}, y_{ir})$ or $(x_{vi}, y_{vi}) \sim P_{\mathcal{V}_g}(x_{vi}, y_{vi})$. To explicitly represent modality information, we transform the data into triplets (x, y, m) , where $m \in \{0, 1\}$; 0 denotes visible modality, and 1 denotes infrared modality.

As shown in Fig.3 (b), stage two learns fusion rules. Input pairs are (x_{ir}, x_{vi}) from image fusion datasets: $(x_{ir}, x_{vi}) \sim P_{\mathcal{I}, \mathcal{V}}(x_{ir}, x_{vi})$.

Stage one uses image restoration datasets, stage two uses an image fusion dataset.

First stage training: In first stage, the unified latent space, \mathcal{Z} , is learned. Image and text encoders extract multi-scale features for both real and pseudo-task data. Given low-quality image x , high-quality image y , text ω , description $c_t = E_{\text{txt}}(\omega)$, pseudo-task text ω_{pd} , pseudo descrip-

tion $c_{pd} = E_{\text{txt}}(\omega_{pd})$, and modality m . We extract latent features: $Z = E_{\text{img}}(x, c_t, m)$ and $Z_{pd} = E_{\text{img}}(y, c_{pd}, m)$ where Z, Z_{pd} are multi-scale latent representations. The decoder reconstructs images: $\hat{y} = D(Z)$ and $\hat{y}_{pd} = D(Z_{pd})$.

The first stage loss \mathcal{L}_1 is formulated as follows:

$$\mathcal{L}_1 = \mathcal{L}_{\text{task}} + \alpha_1^{(1)} \mathcal{L}_{\text{unified}} + \alpha_2^{(1)} \mathcal{L}_{\text{recon}} + \alpha_3^{(1)} \mathcal{L}_{\text{text}}, \quad (4)$$

where

1. $\mathcal{L}_{\text{recon}} = \|\hat{y}_{pd} - y\|_1$ represents the reconstruction loss for the pseudo-degradation task.
2. $\mathcal{L}_{\text{task}} = \|\hat{y} - y\|_1 + \|\|\nabla\hat{y}\| - \|\nabla y\|\|_1$ represents the loss for different degradation tasks (∇ : Sobel operator)
3. $\mathcal{L}_{\text{unified}} = 1 - \Gamma(Z, Z_{pd})$, (Γ : Cosine Similarity)
4. $\alpha_1^{(1)}, \alpha_2^{(1)}, \alpha_3^{(1)}$ are hyperparameters.

Second stage training: In second stage, the proposed model learns fusion rules based on \mathcal{Z} . Given an infrared image x_{ir} , visible image x_{vi} , the pseudo-degradation prompt ω_{pd} and pseudo-degradation task description ($c_{pd} = E_{\text{txt}}(\omega_{pd})$), we extract latent features:

$$Z_{pd}^{\text{ir}} = E_{\text{img}}(x_{ir}, c_{pd}, 1), \quad Z_{pd}^{\text{vi}} = E_{\text{img}}(x_{vi}, c_{pd}, 0). \quad (5)$$

Fusion result O_{fused} is obtained via:

$$O_{\text{fused}} = D\{\text{zero}[F(Z_{pd}^{\text{vi}}, Z_{pd}^{\text{ir}})] + \text{rule}(Z_{pd}^{\text{vi}}, Z_{pd}^{\text{ir}})\}. \quad (6)$$

Inspired by ControlNet [59], we first implement a prior fusion rule, $\text{rule}(\cdot, \cdot)$, for initial feature fusion. A learnable module, $F(\cdot, \cdot)$, then refines rule-based fusion results. A zero-initialized 1×1 convolution mitigates random initialization noise and accelerates Second Stage convergence.

The Second Stage loss function is defined as follows:

$$\mathcal{L}_2 = \mathcal{L}_{\text{color}} + \alpha_1^{(2)} \mathcal{L}_{\text{grad}} + \alpha_2^{(2)} \mathcal{L}_{\text{per}}, \quad (7)$$

where $\alpha_1^{(2)}$ and $\alpha_2^{(2)}$ are hyperparameters balancing loss contributions. Since the proposed unified latent space can extract powerful degradation irrelevant features, theoretically, the fusion loss function not need to be specially designed. Thus, the color consistency item ($\mathcal{L}_{\text{color}}$) and gradient item ($\mathcal{L}_{\text{grad}}$) are chosen from Text-IF [56]. The perceptual item (\mathcal{L}_{per}) is chosen from U2Fusion [53].

3.3.3. Inference

For inference with infrared and visible images (x_{ir}, x_{vi}) and degradation description $c_t = E_{\text{txt}}(\omega)$ and pseudo-degradation $c_{pd} = E_{\text{txt}}(\omega_{pd})$ (assuming infrared is degraded), the process of LURE is given as follows:

$$Z_{pd}^{\text{vi}} = E_{\text{img}}(x_{vi}, c_{pd}, 0), \quad Z_t^{\text{ir}} = E_{\text{img}}(x_{ir}, c_t, 1), \quad (8)$$

$$O_{\text{fused}} = D\{\text{zero}[F(Z_{pd}^{\text{vi}}, Z_t^{\text{ir}})] + \text{rule}(Z_{pd}^{\text{vi}}, Z_t^{\text{ir}})\}. \quad (9)$$

End-to-end inference uses one model, where c_{pd} and c_t denote non-degraded and degraded modalities. This design enables diverse and combined degradation handling via descriptive conditions, without requiring joint degradation training data.

4. Experiment

4.1. Setting

In the proposed model, the encoder and the decoder both consist of 4 layers. The channel numbers for each layer are [48, 96, 192, 384], reduced to [16, 32, 64, 128] for each encoder layer’s output size. K_{bt} and K_{tb} are set to [1,1,2,2] and [2,2,4,8], respectively. Decoder blocks and fusion blocks for each layer is set to [1,1,1,1] and [1, 1, 2, 2]. The number of attention heads for TGA is set to 4, and the prior rule is selected from DenseFuse [24].¹

4.1.1. Training Data

For the first stage of training, we utilize the most common tasks for infrared modality: low contrast (LC) and low resolution (SR) ($\times 4$ and $\times 8$). We use the EMS Full dataset [56] and construct a high-quality super-resolution dataset on LLVIP [17], following the approach in InstructIR [37]. For visible modality, we perform dehazing (HZ), overexposure correction (OE), and low-light enhancement (LL). The high-quality images are chosen from the RESIDE [20], Exposure-Errors [1], and LOL datasets [49], respectively. Our method does not entirely exclude synthetic datasets but reduces reliance on low-quality ones, using real-world and high-quality synthetic restoration data.

For the second stage, the training data of the MSRS datasets [41] is used. All of the aforementioned datasets are publicly available.

All task texts are generated by LLaMA [43].

4.1.2. Evaluation Data

For vanilla image fusion, we evaluate the fusion performance on the RoadScene [54], M3FD [41], TNO [42], and MSRS [41] test dataset.

For degradation-aware image fusion, we use EMS-full [56] for low contrast, overexposure correction, and low-light enhancement. We also construct a super-resolution test dataset on M3FD [41] in the same manner. For dehazing, we collect hazy samples from M3FD [41] to create a real-world dehazing test dataset.

For cross-modal combined degradations, we exemplify with low contrast + overexposure correction and low contrast + low light enhancement, creating combined test datasets from single modality degradation tasks.

¹More detailed hyperparameter (*e.g.* hyperparameter ablation) and training settings are provided in the supplementary materials

4.1.3. Evaluation Metrics

The evaluation metrics include Correlation Coefficient (CC) [13], Spatial Correlation of Differences (SC) [4], Structural Similarity Index (SS) [46], Peak Signal-to-Noise Ratio (PS), Multiscale Structural Similarity (MS) [47], Average Gradient (AG), Standard Deviation (SD), Spatial Frequency (SF), Entropy (EN) [40], CLIP-IQA (CL) [44], LIQE (LI) [60], MANIQA (MA) [55], NIQE (NI) [36], NUSIQ [19] (NU), and ARNIQA (AR) [2].

These metrics comprehensively evaluate the fused image quality from multiple perspectives, including image noise, texture details, and preservation of source image structure. CLIP-IQA [44], LIQE [44], MANIQA [55], NUSIQ [19], and ARNIQA [2] are state-of-the-art no-reference image quality assessment metrics. Except for NIQE, higher values indicate better fusion quality. Red and blue values indicate best and second best results.

4.2. SOTA Competitors

We conducted comparisons against seven state-of-the-art (SOTA) methods, including LRRNet (LRRN) [28], TITA (TITA) [16], SAGE (SAGE) [50], MMDRFuse (MMDR) [12], Text-IF (Text) [56], DAFusion (DAFu) [45], and CDDFuse (CDDF) [63]. Among these, Text-IF and DAFusion are categorized as All-in-One degradation-aware image fusion models. It should be noted that DAFusion (DAFu) is not included for fairness, since it inherently performs restoration on all inputs.

4.3. Vanilla Image Fusion

Table 1. Quantitative comparison of vanilla image fusion task on MSRS and M3FD.

Methods	RoadScene Dataset					MSRS Dataset				
	EN	SC	PS	SS	MS	EN	SC	PS	SS	MS
LRRN’23	7.13	1.57	59.94	0.34	0.49	6.19	0.79	64.74	0.21	0.37
CDDF’23	7.45	1.71	62.14	0.48	0.53	6.70	1.62	64.41	0.50	0.51
MMDR’24	6.51	1.10	62.55	0.41	0.48	6.48	1.53	64.95	0.48	0.52
Text’24	6.64	1.57	62.43	0.48	0.52	6.65	1.68	64.59	0.48	0.52
SAGE’25	7.02	1.52	60.85	0.42	0.51	6.00	1.42	65.28	0.45	0.48
TITA’25	7.09	1.30	63.02	0.49	0.51	6.57	1.61	65.01	0.49	0.52
Ours	7.45	1.67	63.04	0.50	0.55	6.67	1.74	65.12	0.49	0.53

Table 2. Quantitative comparison of vanilla image fusion task on TNO and RoadScene.

Methods	TNO Dataset					M3FD Dataset				
	EN	SC	PS	SS	MS	EN	SC	PS	SS	MS
LRRN’23	6.84	1.62	62.66	0.40	0.43	6.33	1.38	64.14	0.39	0.43
CDDF’23	6.94	1.79	62.43	0.50	0.46	6.75	1.59	62.94	0.52	0.52
MMDR’24	6.31	1.59	62.37	0.48	0.43	6.33	1.40	62.27	0.49	0.50
Text’24	7.04	1.67	62.59	0.47	0.44	6.71	1.41	63.35	0.48	0.48
SAGE’25	6.77	1.79	62.00	0.49	0.45	6.74	1.66	62.69	0.50	0.52
TITA’25	6.70	1.62	62.71	0.51	0.43	6.53	1.33	63.75	0.51	0.50
Ours	6.72	1.84	63.84	0.51	0.47	6.67	1.67	64.24	0.50	0.53

To ensure fair comparison, we first tested degradation-unaware fusion tasks. Quantitative results are in Tab.1

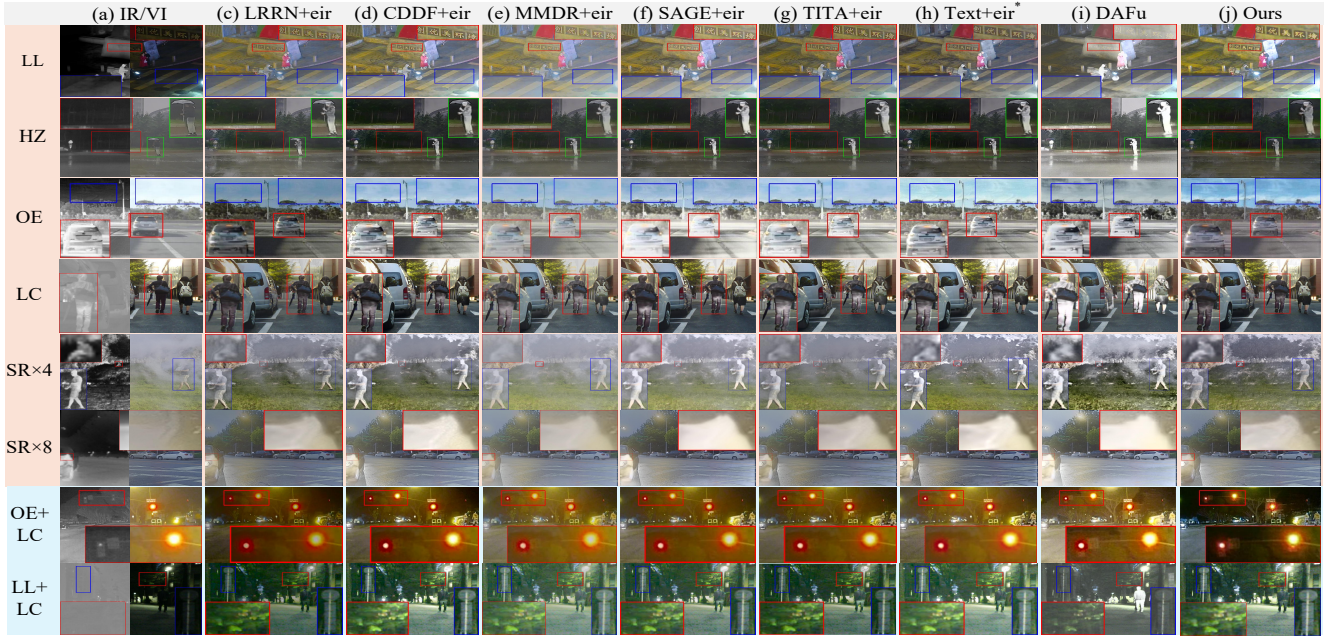


Figure 5. Qualitative comparison of degradation-aware fusion tasks. “eir” denotes External Image Restoration Methods. Text-IF uses “eir” only for Super Resolution and combined degradations. For more detail about the qualitative comparison, please refer to supplementary materials.

and Tab.2. Our method achieves SOTA across all datasets, demonstrating superior performance. Leveraging high-quality image restoration datasets, our method attains higher PS (PSNR), indicating less noisy fusion results. Furthermore, Inner Residuals help preserve more source information, leading to better CC and SC (SCD), and improved SS/MS (SSIM/MS-SSIM), signifying better source information retention and structural fidelity at multiple scales.²

4.4. Degradation-aware Image Fusion

Table 3. Quantitative comparison of degradation-Aware fusion tasks. † denotes All-in-One type methods.

Methods	LL			HZ			OE			LC		
	AG	SD	CL	CL	LI	AR	CL	LI	MA	CL	MA	NI↓
LRRN ²³	3.72	36.41	0.19	0.29	1.07	0.56	0.19	1.24	0.23	0.14	0.17	5.01
CDDF ²³	5.49	50.87	0.18	0.28	1.06	0.54	0.20	1.41	0.25	0.14	0.14	4.25
MMDR ²⁴	3.95	36.07	0.15	0.23	1.17	0.54	0.19	1.23	0.24	0.14	0.14	4.55
SAGE ²⁵	4.73	43.59	0.18	0.28	1.21	0.54	0.20	1.17	0.20	0.15	0.14	4.48
TITA ²⁵	4.93	41.68	0.18	0.29	1.17	0.54	0.18	1.45	0.24	0.14	0.14	6.38
Text ²⁴ †	4.05	42.10	0.19	0.26	1.16	0.54	0.23	1.49	0.23	0.16	0.13	4.41
DAFu ²⁵ †	5.19	47.99	0.19	0.25	1.19	0.52	0.20	1.55	0.24	0.13	0.10	3.17
Ours	4.77	55.23	0.20	0.30	1.14	0.55	0.21	1.37	0.26	0.17	0.15	4.67

Degradation-aware fusion demands models to eliminate degradations and integrate valid source information.

For fair comparison, we use a two-step strategy for degradation-unaware methods: SOTA external image restoration followed by image fusion. For Text-IF’s limitations on some tasks, *e.g.*, super-resolution and combined

²For qualitative evaluation results, due to page limitations, please refer to the supplementary materials.

Table 4. Quantitative comparison of degradation-aware fusion tasks. † denotes All-in-One type methods.

Methods	SR4			SR8			OE+LC			LL+LC		
	SF	CL	AR	SF	CL	AR	EN	AG	CL	EN	SD	CL
LRRN ²³	10.60	0.30	0.59	10.25	0.26	0.58	7.02	4.68	0.20	6.19	31.73	0.14
CDDF ²³	14.00	0.32	0.59	13.54	0.28	0.58	7.47	6.56	0.22	6.70	43.48	0.14
MMDR ²⁴	9.22	0.29	0.59	9.36	0.25	0.57	7.19	4.98	0.21	6.93	37.44	0.10
SAGE ²⁵	11.81	0.26	0.59	11.74	0.23	0.58	7.30	5.74	0.22	5.99	36.26	0.14
TITA ²⁵	12.96	0.30	0.60	12.59	0.26	0.59	7.43	6.13	0.20	7.06	42.66	0.11
Text ²⁴ †	13.20	0.26	0.59	12.78	0.23	0.57	7.51	6.86	0.23	7.26	49.43	0.12
DAFu ²⁵ †	15.23	0.22	0.57	15.23	0.24	0.58	7.47	6.37	0.20	7.24	50.84	0.11
Ours	11.20	0.33	0.60	9.77	0.27	0.59	7.48	6.88	0.24	7.42	55.40	0.15

degradation, we also use this two-stage approach on these tasks. In addition, LRRNet [28], TITA [16], SAGE [50], MMDRFuse [12], and CDDFuse [63] all employ a two-step strategy across tasks. Task-specific SOTA image restoration models: URetinex (LL) [51], SGID-PFF (HZ) [5], CoTF (OE) [31], AirNet (LC) [21], SwinFuSR (SR) [3].³

4.4.1. Qualitative Comparison

Fig.5 qualitatively compare LURE with SOTA methods across degradations, showing LURE’s superiority.

Unlike the existing all-in-One method (DAFusion [45]), LURE benefits from explicit labels as supervisory signals, resulting in richer textural details and less noise in fusion outcomes. Compared to Text-IF [56], our method unconstrained by quadruple data format, leverages more high-quality image restoration datasets with real-world scenar-

³For more information including prompts used in experiments, please refer to supplementary materials.

ios, and yielding more natural images without pre-enhanced sources. Against two-step models like SAGE [50] or MM-DRFuse [12], LURE reduces domain shift-related degradation and information loss.

Crucially, consistent with DAFusion, our method inherently addresses cross-modal combined degradations, achieving superior performance without additional combined degradation training datasets. Text-IF, method-limited, struggles with combined degradations, thus needs external restoration, yielding lower quality. Specifically, for OE+LC and LL+LC tasks, our method exhibits superior detail, color vividness, and contrast compared to other approaches. This shows our method can produce high-quality fused images without extra restoration models.

4.4.2. Quantitative Comparison

Tab.3 and Tab.4 quantitatively compares LURE and SOTA methods across degradations.

LURE generally achieves SOTA performance in 8 tasks. Higher EN, AG, SD, and SF metrics show LURE preserves textural details and clarity. Concurrently, CLIP-IQA (CL), ARNIQA (AR), NUSIQ (NU), MANIQA (MA), LIQE (LI), and NIQE (NI) scores indicate less noise and improved perceptual quality, better aligning with human vision.

4.5. Multi-modal Semantic Segmentation

To assess the effectiveness of LURE in high-level tasks, the experiment of multi-modal semantic segmentation is conducted. Segformer-b2 [52] is fine-tuned on MSRS fusion results and evaluated on the test dataset.⁴

Tab.5 presents mIOU scores, showing LURE achieves SOTA segmentation performance, demonstrating visual efficacy on salient objects. Fig.6 illustrates LURE preserves more texture details than other approaches, enabling more accurate boundary delineation and improved segmentation.

Table 5. Quantitative comparison of multi-modal semantic segmentation on MSRS.

	IR	VI	LRRN	CDDF	MMDR	SAGE	FuB	Text	TITA	Ours
mIOU	63.09	66.81	66.72	67.38	69.11	68.64	67.33	66.26	68.37	69.25

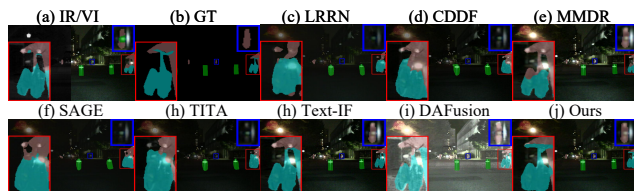


Figure 6. Qualitative comparison of multi-modal semantic segmentation on “00734N” image of MSRS.

⁴For more details please refer to supplementary material.

4.6. Ablation Study

To validate the effectiveness of our method, several ablation studies are conducted (Tab.6), including: Single Stage training, Using CC (vs. Cosine Similarity), w/o Inner Residual, TGA→Gate, w/o Unified Loss and w/o Rule.⁵

Ablation results show Single Stage training caused learning difficulties due to conflicting losses. TGA→Gate substitution impairs spatial information perception from images with text guidance. ‘w/o Unified Loss’ hinders \mathcal{L} learning, significantly degrading fusion quality across tasks.

In remaining ablations, ‘w/o Inner Residual’ makes model prone to high-frequency information loss and convergence issues (minor impact). ‘w/o Rule’ slows Stage Two convergence (moderate impact). Conversely, ‘Using CC’, it provides weaker spatial constraints than Cosine Similarity, caused fusion rule transferability issues.

Table 6. Ablation experiment results.

Configurations	LC			OE			LL+LC		
	CL	MA	NI ↓	CL	LI	MA	EN	SD	CL
Single Stage	0.168	0.135	4.397	0.205	1.041	0.207	6.473	36.901	0.149
Using CC	0.155	0.135	4.828	0.195	1.208	0.216	7.230	48.035	0.134
w/o Inner Residual	0.165	0.138	5.100	0.206	1.310	0.244	7.056	40.099	0.149
TGA→Gate	0.163	0.130	5.000	0.180	1.080	0.200	7.184	45.001	0.143
w/o Unified Loss	0.169	0.139	5.024	0.205	1.030	0.198	7.100	45.829	0.139
w/o Rule	0.159	0.133	5.168	0.203	1.236	0.227	7.053	48.099	0.136
Ours	0.170	0.150	4.671	0.212	1.374	0.259	7.422	55.403	0.152

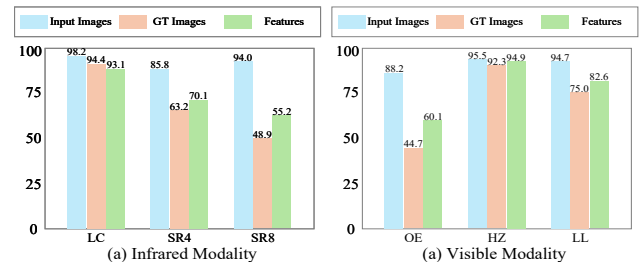


Figure 7. Degradation classification accuracy of three classifiers (Input, GT, ULFS) on IR and VI modalities.

4.7. Validation of Latent Representations

To verify whether ULFS is successfully learned, we train three ResNet-based classifiers using degraded inputs, ground-truth images, and ULFS features from various restoration datasets, respectively. The inputs contain degradation cues, the ground truths retain only dataset-specific scene distributions, while ULFS features are expected to exclude degradation and preserve scene information.

We evaluate all classifiers using ACC. As shown in Fig.7, for both IR and VI, the ULFS-based classifier attains accuracy close to the ground-truth one, indicating that degradation information has been effectively removed and the ULFS space has been effectively approximated.

⁵For more detailed qualitative comparisons and hyperparameter ablation studies, please refer to the supplementary material.

5. Conclusion

This paper addresses limitations of prior ADFMs constrained by long-tailed data, dimensionality curse, and synthetic data reliance. By decoupling modality and quality dimensions at data level and reassociating it at ULFS, our proposed approach mitigates these issues, provides effective supervision, and yields superior fusion performance. Furthermore, an inner residual model enhance spatial perception and detail preservation. Extensive experiments validate our proposed method achieves better performance in vanilla and degradation-aware fusion. Importantly, our method is applicable not only to infrared-visible image fusion but also to other multi-modal image fusion tasks. We believe our approach offers a fresh perspective and inspires future fusion research.

References

- [1] Mahmoud Afifi, Konstantinos G Derpanis, Bjorn Ommer, and Michael S Brown. Learning multi-scale photo exposure correction. In *Proceedings of the IEEE/CVF Conference on Computer Vision and Pattern Recognition*, pages 9157–9167, 2021. 3, 6
- [2] Lorenzo Agnolucci, Leonardo Galteri, Marco Bertini, and Alberto Del Bimbo. Arnika: Learning distortion manifold for image quality assessment. In *Proceedings of the IEEE/CVF Winter Conference on Applications of Computer Vision*, pages 189–198, 2024. 6
- [3] Cyprien Arnold, Philippe Jouvét, and Lama Seoud. Swin-fusr: An image fusion-inspired model for rgb-guided thermal image super-resolution. In *Proceedings of the IEEE/CVF Conference on Computer Vision and Pattern Recognition (CVPR) Workshops*, pages 3027–3036, 2024. 7
- [4] V Aslantas and Emre Bendes. A new image quality metric for image fusion: The sum of the correlations of differences. *Aeu-international Journal of electronics and communications*, 69(12):1890–1896, 2015. 6
- [5] Haoran Bai, Jinshan Pan, Xinguang Xiang, and Jinhui Tang. Self-guided image dehazing using progressive feature fusion. *IEEE Transactions on Image Processing*, 31:1217 – 1229, 2022. 7
- [6] Haowen Bai, Jianshe Zhang, Zixiang Zhao, Yichen Wu, Lilun Deng, Yukun Cui, Tao Feng, and Shuang Xu. Task-driven image fusion with learnable fusion loss. In *Proceedings of the Computer Vision and Pattern Recognition Conference*, pages 7457–7468, 2025. 1
- [7] Liangyu Chen, Xiaojie Chu, Xiangyu Zhang, and Jian Sun. Simple baselines for image restoration. In *European conference on computer vision*, pages 17–33. Springer, 2022. 2, 4, 5
- [8] Xiangyu Chen, Zheyuan Li, Yuandong Pu, Yihao Liu, Jiantao Zhou, Yu Qiao, and Chao Dong. A comparative study of image restoration networks for general backbone network design. *arXiv preprint arXiv:2310.11881*, 2023. 2
- [9] Chunyang Cheng, Tianyang Xu, Xiao-Jun Wu, Hui Li, Xi Li, and Josef Kittler. Fusionbooster: A unified image fusion boosting paradigm. *International Journal of Computer Vision*, pages 1–18, 2024. 1
- [10] Chunyang Cheng, Tianyang Xu, Xiao-Jun Wu, Hui Li, Xi Li, Zhangyong Tang, and Josef Kittler. Textfusion: Unveiling the power of textual semantics for controllable image fusion. *Information Fusion*, 117:102790, 2025. 1
- [11] Marcos V Conde, Gregor Geigle, and Radu Timofte. Instructir: High-quality image restoration following human instructions. In *European Conference on Computer Vision*, pages 1–21. Springer, 2024. 2, 3
- [12] Yanglin Deng, Tianyang Xu, Chunyang Cheng, Xiao-Jun Wu, and Josef Kittler. Mmdrfuse: Distilled mini-model with dynamic refresh for multi-modality image fusion. In *Proceedings of the 32nd ACM International Conference on Multimedia*, pages 7326–7335, 2024. 6, 7, 8
- [13] Manjusha Deshmukh, Udhav Bhosale, et al. Image fusion and image quality assessment of fused images. *International Journal of Image Processing (IJIP)*, 4(5):484, 2010. 6
- [14] Jacob Devlin, Ming-Wei Chang, Kenton Lee, and Kristina Toutanova. Bert: Pre-training of deep bidirectional transformers for language understanding. In *Proceedings of the 2019 conference of the North American chapter of the association for computational linguistics: human language technologies, volume 1 (long and short papers)*, pages 4171–4186, 2019. 4
- [15] Qishen Ha, Kohei Watanabe, Takumi Karasawa, Yoshitaka Ushiku, and Tatsuya Harada. Mfnet: Towards real-time semantic segmentation for autonomous vehicles with multi-spectral scenes. In *IEEE/RSJ International Conference on Intelligent Robots and Systems (IROS)*, pages 5108–5115. IEEE, 2017. 2
- [16] Xingyu Hu, Junjun Jiang, Chenyang Wang, Kui Jiang, Xianning Liu, and Jiayi Ma. Balancing task-invariant interaction and task-specific adaptation for unified image fusion. In *Proceedings of the IEEE/CVF International Conference on Computer Vision*, 2025. 6, 7
- [17] Xinyu Jia, Chuang Zhu, Minzhen Li, Wenqi Tang, and Wenli Zhou. Lvip: A visible-infrared paired dataset for low-light vision. In *Proceedings of the IEEE/CVF International Conference on Computer Vision*, pages 3496–3504, 2021. 2, 6
- [18] Shahid Karim, Geng Tong, Jinyang Li, Akeel Qadir, Umar Farooq, and Yiting Yu. Current advances and future perspectives of image fusion: A comprehensive review. *Information Fusion*, 90:185–217, 2023. 1
- [19] Junjie Ke, Qifei Wang, Yilin Wang, Peyman Milanfar, and Feng Yang. Musiq: Multi-scale image quality transformer. In *Proceedings of the IEEE/CVF international conference on computer vision*, pages 5148–5157, 2021. 6
- [20] Boyi Li, Wenqi Ren, Dengpan Fu, Dacheng Tao, Dan Feng, Wenjun Zeng, and Zhangyang Wang. Benchmarking single-image dehazing and beyond. *IEEE Transactions on Image Processing*, 28(1):492–505, 2019. 2, 3, 6
- [21] Boyun Li, Xiao Liu, Peng Hu, Zhongqin Wu, Jiancheng Lv, and Xi Peng. All-In-One Image Restoration for Unknown Corruption. In *IEEE Conference on Computer Vision and Pattern Recognition*, New Orleans, LA, 2022. 7
- [22] Boyun Li, Xiao Liu, Peng Hu, Zhongqin Wu, Jiancheng Lv, and Xi Peng. All-in-one image restoration for unknown

- corruption. In *Proceedings of the IEEE/CVF conference on computer vision and pattern recognition*, pages 17452–17462, 2022. 2, 3, 4
- [23] Bingchen Li, Xin Li, Yiting Lu, Ruoyu Feng, Mengxi Guo, Shijie Zhao, Li Zhang, and Zhibo Chen. Promptcir: blind compressed image restoration with prompt learning. In *Proceedings of the IEEE/CVF Conference on Computer Vision and Pattern Recognition*, pages 6442–6452, 2024. 3
- [24] Hui Li and Xiao-Jun Wu. Densefuse: A fusion approach to infrared and visible images. *IEEE Transactions on Image Processing*, 28(5):2614–2623, 2018. 2, 6
- [25] Hui Li and Xiao-Jun Wu. Crossfuse: A novel cross attention mechanism based infrared and visible image fusion approach. *Information Fusion*, 103:102147, 2024. 2
- [26] Hui Li, Xiao-Jun Wu, and Tariq Durrani. Nestfuse: An infrared and visible image fusion architecture based on nest connection and spatial/channel attention models. *IEEE Transactions on Instrumentation and Measurement*, 69(12):9645–9656, 2020. 2
- [27] Hui Li, Xiao-Jun Wu, and Josef Kittler. Mdlatrr: A novel decomposition method for infrared and visible image fusion. *IEEE Transactions on Image Processing*, 29:4733–4746, 2020. 1
- [28] Hui Li, Tianyang Xu, Xiao-Jun Wu, Jiwen Lu, and Josef Kittler. Lrrnet: A novel representation learning guided fusion network for infrared and visible images. *IEEE transactions on pattern analysis and machine intelligence*, 45(9):11040–11052, 2023. 6, 7
- [29] Hui Li, Haolong Ma, Chunyang Cheng, Zhongwei Shen, Xiaoning Song, and Xiao-Jun Wu. Conti-fuse: A novel continuous decomposition-based fusion framework for infrared and visible images. *Information Fusion*, 117:102839, 2025. 2
- [30] Xin Li, Bingchen Li, Xin Jin, Cuiling Lan, and Zhibo Chen. Learning distortion invariant representation for image restoration from a causality perspective. In *Proceedings of the IEEE/CVF Conference on Computer Vision and Pattern Recognition*, pages 1714–1724, 2023. 4
- [31] Ziwen Li, Feng Zhang, Meng Cao, Jinpu Zhang, Yuanjie Shao, Yuehuan Wang, and Nong Sang. Real-time exposure correction via collaborative transformations and adaptive sampling. In *Proceedings of the IEEE/CVF Conference on Computer Vision and Pattern Recognition*, pages 2984–2994, 2024. 7
- [32] Pengwei Liang, Junjun Jiang, Xianming Liu, and Jiayi Ma. Fusion from decomposition: A self-supervised decomposition approach for image fusion. In *European Conference on Computer Vision*, pages 719–735. Springer, 2022. 1
- [33] Jinyuan Liu, Xin Fan, Zhanbo Huang, Guanyao Wu, Risheng Liu, Wei Zhong, and Zhongxuan Luo. Target-aware dual adversarial learning and a multi-scenario multi-modality benchmark to fuse infrared and visible for object detection. In *Proceedings of the IEEE/CVF Conference on Computer Vision and Pattern Recognition*, pages 5802–5811, 2022. 2, 3
- [34] Jiayi Ma, Wei Yu, Pengwei Liang, Chang Li, and Junjun Jiang. Fusiongan: A generative adversarial network for infrared and visible image fusion. *Information fusion*, 48:11–26, 2019. 2
- [35] Jiayi Ma, Hao Zhang, Zhenfeng Shao, Pengwei Liang, and Han Xu. Ganmcc: A generative adversarial network with multiclassification constraints for infrared and visible image fusion. *IEEE Transactions on Instrumentation and Measurement*, 70:1–14, 2020. 2
- [36] Anish Mittal, Rajiv Soundararajan, and Alan C Bovik. Making a “completely blind” image quality analyzer. *IEEE Signal processing letters*, 20(3):209–212, 2012. 6
- [37] Hanseok Oh, Hyunji Lee, Seonghyeon Ye, Haebin Shin, Hansol Jang, Changwook Jun, and Minjoon Seo. Instructir: A benchmark for instruction following of information retrieval models. *arXiv preprint arXiv:2402.14334*, 2024. 4, 5, 6
- [38] Yohan Poirier-Ginter and Jean-François Lalonde. Robust unsupervised stylegan image restoration. In *Proceedings of the IEEE/CVF Conference on Computer Vision and Pattern Recognition*, pages 22292–22301, 2023. 4
- [39] Alec Radford, Jong Wook Kim, Chris Hallacy, Aditya Ramesh, Gabriel Goh, Sandhini Agarwal, Girish Sastry, Amanda Askell, Pamela Mishkin, Jack Clark, et al. Learning transferable visual models from natural language supervision. In *International conference on machine learning*, pages 8748–8763. PmLR, 2021. 4
- [40] J Wesley Roberts, Jan A Van Aardt, and Fethi Babikker Ahmed. Assessment of image fusion procedures using entropy, image quality, and multispectral classification. *Journal of Applied Remote Sensing*, 2(1):023522, 2008. 6
- [41] Linfeng Tang, Jiteng Yuan, Hao Zhang, Xingyu Jiang, and Jiayi Ma. Piafusion: A progressive infrared and visible image fusion network based on illumination aware. *Information Fusion*, 2022. 2, 3, 6
- [42] Alexander Toet. Tno image fusion dataset. *figshare*, 2024. 6
- [43] Hugo Touvron, Thibaut Lavril, Gautier Izacard, Xavier Martinet, Marie-Anne Lachaux, Timothée Lacroix, Baptiste Rozière, Naman Goyal, Eric Hambro, Faisal Azhar, et al. Llama: Open and efficient foundation language models. *arXiv preprint arXiv:2302.13971*, 2023. 6
- [44] Jianyi Wang, Kelvin CK Chan, and Chen Change Loy. Exploring clip for assessing the look and feel of images. In *Proceedings of the AAAI conference on artificial intelligence*, pages 2555–2563, 2023. 6
- [45] Xue Wang, Zheng Guan, Wenhua Qian, Jinde Cao, Runzhuo Ma, and Cong Bi. A degradation-aware guided fusion network for infrared and visible image. *Information Fusion*, 118:102931, 2025. 3, 6, 7
- [46] Zhou Wang and Alan C Bovik. A universal image quality index. *IEEE signal processing letters*, 9(3):81–84, 2002. 6
- [47] Zhou Wang, Eero P Simoncelli, and Alan C Bovik. Multiscale structural similarity for image quality assessment. In *The Thirty-Seventh Asilomar Conference on Signals, Systems & Computers, 2003*, pages 1398–1402. Ieee, 2003. 6
- [48] Zeyu Wang, Jizheng Zhang, Haiyu Song, Mingyu Ge, Jiayu Wang, and Haoran Duan. Highlight what you want: Weakly-supervised instance-level controllable infrared-visible image fusion. In *Proceedings of the IEEE/CVF International Conference on Computer Vision*, pages 12637–12647, 2025. 2

- [49] Chen Wei, Wenjing Wang, Wenhan Yang, and Jiaying Liu. Deep retinex decomposition for low-light enhancement. *arXiv preprint arXiv:1808.04560*, 2018. 2, 3, 6
- [50] Guanyao Wu, Haoyu Liu, Hongming Fu, Yichuan Peng, Jinyuan Liu, Xin Fan, and Risheng Liu. Every sam drop counts: Embracing semantic priors for multi-modality image fusion and beyond. In *Proceedings of the Computer Vision and Pattern Recognition Conference*, pages 17882–17891, 2025. 6, 7, 8
- [51] Wenhui Wu, Jian Weng, Pingping Zhang, Xu Wang, Wenhan Yang, and Jianmin Jiang. Uretinex-net: Retinex-based deep unfolding network for low-light image enhancement. In *Proceedings of the IEEE/CVF conference on computer vision and pattern recognition*, pages 5901–5910, 2022. 7
- [52] Enze Xie, Wenhai Wang, Zhiding Yu, Anima Anandkumar, Jose M Alvarez, and Ping Luo. Segformer: Simple and efficient design for semantic segmentation with transformers. *Advances in neural information processing systems*, 34: 12077–12090, 2021. 8
- [53] Han Xu, Jiayi Ma, Junjun Jiang, Xiaojie Guo, and Haibin Ling. U2fusion: A unified unsupervised image fusion network. *IEEE transactions on pattern analysis and machine intelligence*, 44(1):502–518, 2020. 2, 5
- [54] Han Xu, Jiayi Ma, Zhuliang Le, Junjun Jiang, and Xiaojie Guo. Fusiondn: A unified densely connected network for image fusion. In *proceedings of the Thirty-Fourth AAAI Conference on Artificial Intelligence*, 2020. 2, 3, 6
- [55] Sidi Yang, Tianhe Wu, Shuwei Shi, Shanshan Lao, Yuan Gong, Mingdeng Cao, Jiahao Wang, and Yujiu Yang. Maniqa: Multi-dimension attention network for no-reference image quality assessment. In *Proceedings of the IEEE/CVF Conference on Computer Vision and Pattern Recognition*, pages 1191–1200, 2022. 6
- [56] Xunpeng Yi, Han Xu, Hao Zhang, Linfeng Tang, and Jiayi Ma. Text-if: Leveraging semantic text guidance for degradation-aware and interactive image fusion. In *Proceedings of the IEEE/CVF Conference on Computer Vision and Pattern Recognition*, pages 27026–27035, 2024. 1, 2, 3, 5, 6, 7
- [57] Syed Waqas Zamir, Aditya Arora, Salman Khan, Munawar Hayat, Fahad Shahbaz Khan, and Ming-Hsuan Yang. Restormer: Efficient transformer for high-resolution image restoration. In *Proceedings of the IEEE/CVF conference on computer vision and pattern recognition*, pages 5728–5739, 2022. 2, 4, 5
- [58] Hao Zhang, Han Xu, Xin Tian, Junjun Jiang, and Jiayi Ma. Image fusion meets deep learning: A survey and perspective. *Information Fusion*, 76:323–336, 2021. 1
- [59] Lvmin Zhang, Anyi Rao, and Maneesh Agrawala. Adding conditional control to text-to-image diffusion models. In *Proceedings of the IEEE/CVF international conference on computer vision*, pages 3836–3847, 2023. 5
- [60] Weixia Zhang, Guangtao Zhai, Ying Wei, Xiaokang Yang, and Kede Ma. Blind image quality assessment via vision-language correspondence: A multitask learning perspective. In *IEEE Conference on Computer Vision and Pattern Recognition*, pages 14071–14081, 2023. 6
- [61] Zeyang Zhang, Hui Li, Tianyang Xu, Xiao-Jun Wu, and Josef Kittler. Ddbfusion: An unified image decomposition and fusion framework based on dual decomposition and bézier curves. *Information Fusion*, 114:102655, 2025. 1
- [62] Wenda Zhao, Shigeng Xie, Fan Zhao, You He, and Huchuan Lu. Metafusion: Infrared and visible image fusion via meta-feature embedding from object detection. In *Proceedings of the IEEE/CVF Conference on Computer Vision and Pattern Recognition*, pages 13955–13965, 2023. 1
- [63] Zixiang Zhao, Haowen Bai, Jianshe Zhang, Yulun Zhang, Shuang Xu, Zudi Lin, Radu Timofte, and Luc Van Gool. Cddfuse: Correlation-driven dual-branch feature decomposition for multi-modality image fusion. In *Proceedings of the IEEE/CVF conference on computer vision and pattern recognition*, pages 5906–5916, 2023. 2, 6, 7
- [64] Zixiang Zhao, Haowen Bai, Yuanzhi Zhu, Jianshe Zhang, Shuang Xu, Yulun Zhang, Kai Zhang, Deyu Meng, Radu Timofte, and Luc Van Gool. Ddfm: denoising diffusion model for multi-modality image fusion. In *Proceedings of the IEEE/CVF International Conference on Computer Vision*, pages 8082–8093, 2023. 2